frontiers in Marine Science

TYPE Original Research
PUBLISHED 22 June 2026
DOI 10.3389/fmars.2026.1843359

Check for updates

OPEN ACCESS

EDITED BY
Paolo Magni,
National Research Council (CNR), Italy

REVIEWED BY
Patricia Wiberg,
University of Virginia, United States
Yuzheng Ren,
State Oceanic Administration, China

*CORRESPONDENCE
Jie Liu
chaoshuiliujie@163.com

RECEIVED 31 March 2026
REVISED 21 May 2026
ACCEPTED 28 May 2026
PUBLISHED 22 June 2026

CITATION
Chen L, Liu X, Zhu A, Wang X and Liu J (2026) Seasonal dynamics of seagrass-mediated sediment stabilization in a temperate eelgrass meadow: field evidence from the Yellow Sea. *Front. Mar. Sci.* 13:1843359. doi: 10.3389/fmars.2026.1843359

COPYRIGHT
© 2026 Chen, Liu, Zhu, Wang and Liu. This is an open-access article distributed under the terms of the Creative Commons Attribution License (CC BY). The use, distribution or reproduction in other forums is permitted, provided the original author(s) and the copyright owner(s) are credited and that the original publication in this journal is cited, in accordance with accepted academic practice. No use, distribution or reproduction is permitted which does not comply with these terms.

Seasonal dynamics of seagrass-mediated sediment stabilization in a temperate eelgrass meadow: field evidence from the Yellow Sea

Lu Chen[1], Xiaohui Liu[2], Ancheng Zhu[2], Xitao Wang[2] and Jie Liu[2]*

[1]College of Marine Life Sciences, Ocean University of China, Qingdao, Shandong, China, [2]Planning and Sea Island Department, Shandong Marine Forecast and Hazard Mitigation Service, Qingdao, Shandong, China

Seagrass meadows stabilize coastal sediment through canopy attenuation of hydrodynamic forces and rhizome mechanical anchoring, yet the full-year temporal dynamics of this effect across contrasting hydrodynamic conditions remain poorly documented, and static cross-sectional designs cannot distinguish seagrass actively driving sediment change from fine-grained substrates passively attracting colonization. We conducted 14 consecutive months of monthly paired field observations at three *Zostera marina* sites along a hydrodynamic exposure gradient in the Yellow Sea, China, tracking seagrass biomass, sediment properties, surface elevation, and water optical environment, with hydrodynamic intensity and benthic microalgal biomass controlled as covariates in linear mixed-effects models. The difference in median grain size between vegetated and bare areas (ΔD50) tracked the seasonal rhythm of aboveground biomass strictly, with summer peaks of 55, 47, and 29 μm and winter minima of 17, 13, and 11 μm at the low-, intermediate-, and high-energy sites; the treatment effect changed by approximately 5% after covariate control. This strict temporal coupling supports seagrass actively driving sediment stabilization rather than passively colonizing fine-grained substrates. A non-zero winter residual ΔD50 coincided with below-ground biomass remaining at 75–80% of peak values, indicating that rhizome anchoring maintains baseline stabilization independently after canopy senescence. Cumulative elevation confirmed this pattern, with net deposition of +11 mm at the low-energy vegetated site versus net erosion of −9 mm at the high-energy bare site. Water transparency differences correlated strongly with leaf area index (R^2 = 0.77–0.89, $p < 0.001$), demonstrating that sediment stabilization simultaneously improves the benthic light environment. The seasonal amplitude of stabilization decreased with increasing hydrodynamic exposure, while winter erosion vulnerability was greatest at the high-energy site. These findings advance causal attribution of seagrass sediment stabilization from static association to temporal-dynamics-level evidence, and provide a basis for temporally targeted conservation — particularly restricting anthropogenic disturbance during winter at high-exposure meadows.

KEYWORDS
hydrodynamic exposure gradient, seasonal dynamics, sediment stabilization, water transparency, *Zostera marina*

1 Introduction

Seagrass meadows rank among the most productive coastal ecosystems on Earth, with a documented global distribution area of approximately 267,000 km^2 (McKenzie et al., 2020). They provide substantial ecosystem services, including blue carbon sequestration, habitat provisioning, and the support of commercially important fisheries resources (Lima et al., 2023). However, the cumulative effects of coastal eutrophication, physical disturbance, coastal development, and climate change have driven a loss of approximately one-fifth (19.1%) of global seagrass area since the late nineteenth century, and decline continues across multiple biogeographic regions (Dunic et al., 2021). Coastal seagrass beds in China face similarly severe threats: for example, the iconic *Zostera marina* meadow at Caofeidian in the Bohai Sea has experienced dramatic contraction under land reclamation and other anthropogenic pressures, though satellite monitoring also documents substantial recovery to near-peak levels by 2019 (Xu et al., 2021), and habitat suitability modelling indicates that suitable *Z. marina* habitat across the northern Chinese seas is subject to constraints from multiple environmental factors and human activities (Wang et al., 2024). Among the key physical processes that enable seagrass meadows to sustain themselves, sediment stabilization is of particular importance: seagrass loss can weaken this function and trigger cascading degradation of habitat conditions (van der Heide et al., 2007; Maxwell et al., 2017). Understanding the magnitude and temporal dynamics of sediment stabilization is therefore fundamental to assessing meadow vulnerability and developing effective conservation strategies.

Seagrass meadows stabilize sediment through two complementary pathways. Seagrasses attenuate wave energy and reduce near-bed flow velocities through their leaf canopies, thereby suppressing sediment resuspension and promoting the deposition of suspended particles (Reidenbach and Thomas, 2018; Hansen and Reidenbach, 2013). Belowground root–rhizome networks simultaneously enhance substrate resistance to erosion through mechanical anchoring (Marin-Diaz et al., 2020; Infantes et al., 2022). Together, these two pathways reduce water-column SPM concentrations and improve benthic light availability — the primary environmental factor limiting the distribution of temperate seagrasses (Léger-Daigle et al., 2022). Quantifying the magnitude and temporal dynamics of this sediment stabilization effect across seasons is therefore fundamental to evaluating meadow ecological function and identifying periods of heightened vulnerability.

Considerable mechanistic understanding of seagrass-mediated sediment stabilization has accumulated for both canopy hydrodynamic attenuation and rhizome mechanical anchoring, and this understanding has been broadly validated in flume experiments and field measurements (Reidenbach and Thomas, 2018; Marin-Diaz et al., 2020; Infantes et al., 2022). Regarding the canopy pathway, field measurements by Reidenbach and Thomas (2018) along the Virginia coast showed that *Z. marina* canopies reduced significant wave height by 25–49%, and near-bed shear stress remained consistently below the critical resuspension threshold throughout the summer high-density period while simultaneously exceeding it at adjacent bare sites. Regarding the rhizome pathway, flume experiments by Marin-Diaz et al. (2020) demonstrated that rhizome networks reduced bedload transport by approximately 50%, and Infantes et al. (2022) directly measured reductions in lateral sediment erosion rates of up to 70% attributable to root systems, with both studies explicitly noting that rhizome effects operate independently of the aboveground canopy. Additionally, benthic microalgae can independently provide sediment stabilization by forming biofilms on the sediment surface; this contribution must be treated as a confounding factor when investigating seagrass-mediated stabilization effects (Reidenbach and Timmerman, 2019).

However, most existing studies have employed static cross-sectional designs — comparing sediment properties between vegetated and bare areas at a single point in time (Bos et al., 2007; Ganthy et al., 2013; Potouroglou et al., 2017). This design has a fundamental limitation: a single cross-sectional observation cannot distinguish between "seagrass actively stabilizing sediment" and "fine-grained substrate attracting seagrass colonization" — two opposite causal directions (van der Heide et al., 2007). Indeed, evidence from other systems suggests that seagrasses may preferentially colonize sandy rather than fine-grained substrates (Koch, 2001; Murphy et al., 2011), weakening the plausibility of the passive-selection hypothesis. Nevertheless, the inability of static designs to resolve temporal directionality remains a genuine methodological limitation, regardless of which alternative hypothesis is considered. Advancing this causal inference within an observational framework requires tracking the temporal dynamics of stabilization effects as seagrass biomass changes across seasons. If the difference in sediment properties between vegetated and bare areas follows the seasonal rhythm of biomass continuously and strictly, the reverse explanation — that substrate passively selects for seagrass — becomes untenable, and the direction of seagrass actively driving sediment change receives support. Yet almost no studies have systematically tracked the full annual temporal dynamics of this effect, and the methodological limitations of static cross-sectional designs mean that causal attribution of sediment stabilization effects has lacked effective testing at the level of temporal dynamics (Hansen and Reidenbach, 2013; Ganthy et al., 2013; Potouroglou et al., 2017).

Temperate seagrass meadows exhibit highly regular seasonal oscillations in aboveground biomass, with leaf biomass approaching complete senescence in winter and reaching a summer peak, with oscillation amplitudes exceeding one order of magnitude (Zhang et al., 2016). If seagrass genuinely drives sediment stabilization actively, this biomass rhythm should leave a clear imprint on the temporal dynamics of sediment properties, with effect intensity varying continuously with seasonal biomass change (Zhu et al., 2021; Zhu et al., 2022). Existing studies have provided scattered evidence at discrete temporal nodes. Hansen and Reidenbach (2013) conducted four-season continuous monitoring along the Virginia coast and found that canopy suppression of near-bed shear stress was strongest in summer and markedly weaker in winter, indicating that effect intensity varies systematically with seasonal biomass oscillations — yet their study covered only flow velocity and suspended particles without tracking the full-year continuous dynamics of sediment grain size and surface elevation. Ganthy et al. (2013) conducted year-round high-frequency bed-level monitoring

in Arcachon Bay, France, and found sustained net accumulation in vegetated areas during the growing season with a tendency toward reversal during senescence. Potouroglou et al. (2017) recorded mean annual elevation differences of 31 mm between vegetated and bare areas in perennial *Z. marina* meadows in Scotland, noting that measurable stabilization effects persisted even during winter when aboveground biomass was sparse. However, none of these studies provided systematic evidence of effect intensity oscillating continuously throughout the full seasonal biomass rhythm — either because results were aggregated as annual means or because only a few seasonal snapshots were captured. The relative contributions and seasonal interaction of canopy effects and rhizome effects also lack direct testing through full-year tracking data. Whether the improvement in water-column SPM concentration and transparency associated with sediment stabilization effects undergoes a simultaneous seasonal variation — forming an observable sediment–light coupled seasonal response — similarly awaits validation from full-year tracking data. Clarifying these dynamics has direct relevance for assessing the intensity of meadow ecological function at different points within the annual cycle and for identifying periods of heightened vulnerability.

Under contrasting hydrodynamic exposure conditions, high-energy environments may systematically limit the maximum attainable intensity of canopy stabilization effects by constraining the upper limit of seagrass biomass accumulation (Dahl et al., 2020; de Smit et al., 2022). *In situ* flume experiments by de Smit et al. (2022) demonstrated a linear positive relationship between the critical flow velocity for *Z. marina* sediment resuspension and leaf area, such that biomass limitation at high-energy sites directly compresses the effect ceiling. A systematic survey of 53 *Z. marina* meadows along the Swedish Skagerrak coast by Dahl et al. (2020) further revealed that the dominant stabilization mechanism shifts from fine-particle trapping in sheltered environments to substrate compaction and erosion resistance in exposed environments — a mechanistic distinction of fundamental nature. Meanwhile, the external erosive driving force is stronger in high-energy environments, meaning that geomorphic losses following meadow degradation to bare substrate may far exceed those in low-energy environments. Research by El-Hacen et al. (2019) across an exposure gradient in Mauritania indicated stronger coupling between geomorphic stability and vegetation cover state at high-exposure sites, where any cover loss may trigger a state shift beyond a critical threshold (Maxwell et al., 2017). The superposition of these two aspects implies that seasonal variation in stabilization effects not only differs in amplitude across hydrodynamic gradients but may also amplify in ecological consequence with increasing exposure. Yet virtually all existing studies have been conducted under a single hydrodynamic background, and while the numerical modelling study of Mohr et al. (2025) and field observations by Zhu et al. (2021, 2022) pointed out that seasonal variation in seagrass properties exerts a non-negligible regulatory effect on hydro-morphodynamic processes, systematic field research comparing seasonal dynamics of stabilization effects across hydrodynamic exposure gradients remains absent.

The present study focused on a temperate *Zostera marina* meadow in the Yellow Sea, China. Monthly paired field observations were conducted over 14 consecutive months at three sites distributed along a hydrodynamic exposure gradient (low-energy, intermediate-energy, and high-energy), simultaneously tracking the temporal dynamics of seagrass biomass, sediment grain size and surface elevation, water SPM concentration, and water transparency. Gypsum dissolution rates and benthic chlorophyll a content served as control covariates for hydrodynamic intensity and benthic microalgal effects, respectively. The aims of this study were to: (1) quantify the continuous variation in the sediment difference between vegetated and bare areas with the seasonal rhythm of *Z. marina* biomass, and provide temporal-dynamics-level observational evidence — after controlling for physical background and microalgal effects — for seagrass actively driving sediment stabilization; (2) evaluate whether seasonal variation in sediment stabilization effects is simultaneously reflected in improvements to the water optical environment; and (3) compare differences in the seasonal amplitude of these effects across sites of contrasting hydrodynamic exposure, and assess the geomorphic vulnerability of the high-energy site during winter. The results provide empirical evidence for assessing the intensity of temperate seagrass meadow ecological function at different points within the annual cycle, and offer scientific reference for identifying highly vulnerable meadow types and optimizing the temporal management of nearshore human activities.

2 Materials and methods

2.1 Study area

Fieldwork was conducted in coastal waters near Qingdao City, Shandong Province, China (35°–36°30′N, 120°–121°E). Qingdao has a temperate monsoon climate, with a mean annual air temperature of 12.3 °C and sea surface temperatures ranging from −1 °C (February) to 26 °C (August). The tidal regime is regular semidiurnal, with a maximum tidal range of 2.78 m. The western Yellow Sea is dominated by northwesterly monsoons in winter and southwesterly monsoons in summer, generating pronounced seasonal differences in hydrodynamic conditions that provided a natural hydrodynamic gradient background for this study. The *Z. marina* population near Qingdao is a typical temperate seasonal assemblage: rapid growth commences in spring (March), aboveground biomass peaks in July–August, leaves progressively senesce in autumn, and only rhizomes overwinter.

Three study sites were selected (Figure 1, Table 1) along a hydrodynamic exposure gradient. S1 was located on the inner side of Jiaozhou Bay, a low-energy, tidal-current-dominated environment with significant wave heights (Hs) typically below 0.3 m and a silt–fine-sand substrate. S2 was located in Huiquan Bay, an intermediate-energy semi-enclosed environment with Hs of 0.3–0.8 m and a fine-sand substrate. S3 was located on the northern side of Laoshan Bay, a high-energy open bay with Hs exceeding 0.8 m during the northwesterly monsoon season in winter and a medium-sand substrate. Water depths at all three sites ranged from 0.5 to 4.0 m, and all had documented stable *Z. marina* populations.

The tidal regime at all three sites is regular semidiurnal, with a maximum tidal range of 2.78 m. Depth-averaged tidal current velocities range from 0.1–0.3 m s^{-1} at S1, 0.2–0.5 m s^{-1} at S2, and

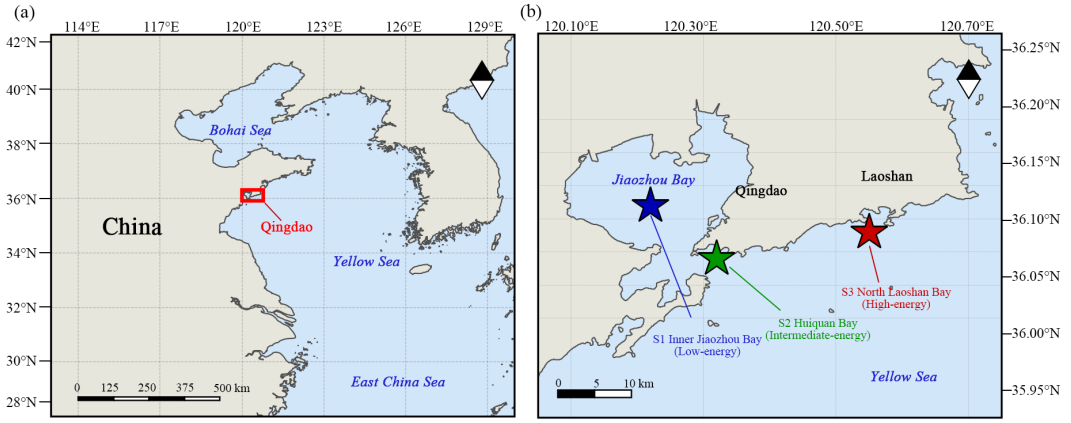


FIGURE 1
Location of the three study sites in the Yellow Sea, China. **(a)** Regional map showing the position of Qingdao on the eastern coast of China. **(b)** Enlarged map showing the three sampling sites: S1 (Inner Jiaozhou Bay, low-energy), S2 (Huiquan Bay, intermediate-energy), and S3 (North Laoshan Bay, high-energy).

0.3–0.7 m s^{-1} at S3. At the low-energy S1 site, tidal currents are the primary driver of near-bed hydrodynamic forcing, whereas at the intermediate-energy S2 and high-energy S3 sites, wind-generated waves become the dominant driver of sediment resuspension, particularly during the northwesterly monsoon season in winter. The wind environment in the study area is strongly seasonal: winter months (November–February) are dominated by northwesterly monsoons with mean monthly wind speeds of 5.5–6.8 m s^{-1}, while summer months (June–August) are characterized by weaker southwesterly winds with mean monthly wind speeds of 3.1–4.0 m s^{-1} (Supplementary Table S1). Wind speed data were obtained from the Qingdao Meteorological Observatory.

2.2 Experimental design

Sampling commenced in March 2024 (one month prior to spring growth initiation) and continued for 14 consecutive months through April of the following year, encompassing a complete annual cycle with boundary buffer months. Monthly sampling was conducted on 14 occasions, covering the pre-growth period (March), rapid growth phase (April–May), peak biomass period (June–August), senescence phase (September–October), dormancy period (November–February of the following year), and the onset of recovery (March–April of the following year). At each site, five fixed replicate sampling points were established in both the vegetated and bare areas, with paired distances not exceeding 10 m to ensure that both zones were exposed to similar hydrodynamic and substrate background conditions. All sampling points were marked with PVC stakes and recorded with GPS coordinates; the same fixed locations were revisited each month to track temporal dynamics of sediment properties at the same points. Bare areas were selected to be comparable in water depth and substrate type to the vegetated areas but without seagrass cover.

2.3 Measured variables

Seagrass metrics served as the primary driver variables. Each month, a 0.25 m^2 PVC quadrat frame was placed at each vegetated sampling point. All shoots within the quadrat were counted to determine shoot density (shoots m^2), and 10 shoots were randomly selected for leaf length and width measurements; shoot density and leaf dimensions were combined to calculate leaf area index (LAI, m^2 m^{-2}). Destructive sampling for biomass estimation was conducted quarterly (March, June, September, December, and April of the following year) at locations independent of the monitoring quadrats (n = 3 replicate quadrats per site). Aboveground leaves were clipped and belowground rhizomes were excavated to 15 cm depth; samples were rinsed, oven-dried at 65 °C for 48 h, and weighed to determine aboveground and belowground dry biomass (g DW m^{-2}), respectively.

TABLE 1 Basic characteristics of the three study sites.

Site	Location	Hydrodynamic characteristics	Substrate type	Mean water depth (m)	Mean tidal range (m)
S1	Inner Jiaozhou Bay	Low-energy, tidal-current-dominated, mean Hs < 0.3 m	Silt–fine sand	0.92	1.5
S2	Huiquan Bay	Intermediate-energy, semi-enclosed, mean Hs 0.3–0.8 m	Fine sand	1.56	2.0
S3	North Laoshan Bay	High-energy, open, mean Hs > 0.8 m (winter)	Medium sand	2.24	2.5

Hs = annual mean significant wave height; mean water depth is relative to mean sea level; mean tidal range is the difference between mean high water and mean low water. Monthly water surface elevation time series and regional wind conditions during the 14-month sampling period are provided in Supplementary Tables S1 and S2.

Sediment metrics constituted the primary response variables. Each month, sediment cores were collected at each of the five fixed replicate points in both the vegetated and bare areas using a PVC tube with an inner diameter of 3 cm, sampling the uppermost 0–5 cm of surface sediment. To avoid cumulative disturbance from repeated coring, each core was taken immediately adjacent to the PVC stake marker at a position not previously sampled. After removing biotic debris, grain size distributions were determined using a laser diffraction particle size analyzer, yielding multiple grain size parameters including median grain size (D50, μm), the percentage of fine particles (<63 μm), and the sorting coefficient; D50 was used as the primary response variable in all statistical analyses, as it most directly reflects the net balance between fine-particle deposition and coarse-particle resuspension driven by canopy hydrodynamic effects. In addition, three 1 m-long stainless steel rods were installed in both vegetated and bare areas at each site as surface elevation change pins (SECPs) (Potouroglou et al., 2017). To minimize potential scour effects around the rods, SECPs were installed at least three months prior to the first measurement to allow the surrounding sediment to equilibrate. Each measurement was taken at a distance of 15 cm from the rod to avoid the localized scour zone. Rod positions were inspected monthly, and no significant scour features were observed around vegetated-area rods during the study period. At bare sites, minor scour depressions (< 5 mm depth) were occasionally observed immediately adjacent to the rods following storm events but did not extend to the measurement distance. Site-specific sediment bulk density was not measured; surface elevation changes therefore represent vertical accretion or erosion rather than mass fluxes, which is acknowledged as a limitation (see Section 4). The exposed height above the sediment surface was recorded monthly, and the difference between successive measurements was used to quantify the monthly net deposition or net erosion rate, providing direct geomorphic evidence.

Water column metrics were used to test whether the seagrass sediment stabilization effect simultaneously improved the water optical environment. All water sampling and Secchi depth measurements were conducted during mid-flood to high tide under calm weather conditions (wind speed < 5 m s^{-1}, no precipitation) to ensure comparability across months and sites. Sampling at all three sites was completed within the same tidal cycle on each monthly survey date. Water temperature was recorded concurrently at each site using a handheld multiparameter probe. Water temperatures were similar across the three sites on each sampling date (mean difference < 0.5 °C), consistent with their location within the same coastal region and similar depth range, and exhibited a typical seasonal cycle ranging from 3.2 °C in January to 26.8 °C in August. At each monthly sampling occasion, Secchi depth was measured both within the vegetated area and alongside the bare area (recorded as the mean of the disappearance and reappearance depths). In addition, 500 mL water samples were collected from both locations, filtered through pre-weighed GF/F glass-fibre filters, dried at 105 °C, and reweighed to calculate SPM concentration (mg L^{-1}). Differences in Secchi depth and SPM concentration between vegetated and bare areas served as quantitative indices of the improvement in the water optical environment.

Hydrodynamic proxy metrics were a critical design element for controlling the confounding effects of seasonal variation in physical forcing. Each month, two standardised cylindrical gypsum dissolution tablets (3 cm diameter × 4 cm height) were deployed in both the vegetated and bare areas at each site, fixed 10 cm above the sediment surface, replaced monthly, and weighed to determine the dissolution rate (g d^{-1}). The gypsum dissolution rate is positively correlated with near-bottom water motion intensity and served as a relative proxy for monthly mean hydrodynamic intensity.

Benthic microalgal metrics were measured to exclude confounding explanations. Benthic diatoms can stabilize sediment independently by forming biofilms on the sediment surface, and their biomass exhibits some degree of seasonality. Each month, the extreme surface layer (0–5 mm) of sediment was collected, frozen in liquid nitrogen, extracted in 90% acetone for 24 h, and quantified spectrophotometrically (at 665 and 750 nm) for benthic chlorophyll a content. Total extracted chlorophyll a was normalized to the core cross-sectional area ($\pi \times 1.5^2 \approx 7.07$ cm^2) and expressed as areal concentration (mg m^{-2}).

2.4 Statistical analysis

Prior to the main analysis, Pearson correlation tests between gypsum dissolution rates and mean monthly wind speed were conducted to validate the effectiveness of the hydrodynamic proxy. Benthic chlorophyll a content was included as a covariate in LMMs to control for the independent contribution of benthic microalgae to sediment stabilization. The core analysis used linear mixed-effects models (LMMs) to test whether the seagrass sediment stabilization effect on D50 varied systematically with season. LMMs were fitted using the lme4 package (Bates et al., 2015) in R version 4.3.2 (R Core Team, 2023). Prior to model fitting, all continuous variables were centred and scaled to facilitate comparison of effect sizes. Model assumptions were verified by inspection of residual plots: normality of residuals was assessed using Q–Q plots and the Shapiro–Wilk test, and homoscedasticity was evaluated by plotting residuals against fitted values. Model fit was assessed using marginal R^2 (variance explained by fixed effects) and conditional R^2 (variance explained by both fixed and random effects), calculated via the MuMIn package (Bartoń, 2023). Estimated marginal means were computed using the emmeans package (Lenth, 2023). Fixed effects included treatment (vegetated/bare), month, their interaction, and two covariates: gypsum dissolution rate and benthic chlorophyll a. Because the fixed-location repeated-measures design generates temporal autocorrelation between observations at the same sampling point in adjacent months, a random intercept term (1|site: replicate) was included to account for this non-independence; a site intercept (1|site) controlled background differences among the three sites. The critical test was the treatment × month interaction: a significant positive interaction (greater vegetated–bare differences in summer than in winter) would support the expectation that stabilization effects vary with seasonal biomass oscillations.

Prior to parametric testing, all variables were assessed for normality using the Shapiro–Wilk test, and homogeneity of variance was evaluated using Levene's test. Variables that did not meet the normality assumption were log-transformed before analysis.

Whether improvement in the water optical environment was synchronous with the sediment stabilization effect in vegetated areas was assessed using a two-step analysis: first, paired t-tests were applied to test whether monthly differences in Secchi depth between vegetated and bare areas were statistically significant; second, Pearson correlation analysis was used to examine the relationship between monthly mean LAI and the transparency difference (vegetated minus bare). Site × month interaction effects were used to test the moderating influence of hydrodynamic exposure gradient on the seasonal amplitude of stabilization effects.

3 Results

3.1 Seasonal dynamics of seagrass biomass

All three sites exhibited pronounced seasonal growth rhythms in *Z. marina* (Figure 2). Aboveground biomass peaked in summer (June–August), reaching 105, 85, and 62 g DW m^{-2} at S1, S2, and S3, respectively, before declining rapidly to annual minima in December (S1: 8 g DW m^{-2}; S2: 6 g DW m^{-2}; S3: 5 g DW m^{-2}), representing a seasonal oscillation amplitude exceeding tenfold. Belowground biomass exhibited a much smaller seasonal amplitude than the aboveground component, peaking in September (S1: 190 g DW m^{-2}; S2: 155 g DW m^{-2}; S3: 115 g DW m^{-2}), lagging the aboveground peak by approximately 1–2 months, and declining to winter minima that still maintained 75–80% of peak values. Shoot density and LAI followed the same seasonal trajectory as aboveground biomass, both reaching maximum values in July–August (Figure 2a). A clear gradient in biomass was evident among the three sites: absolute values of all indices at S1 consistently exceeded those at S2 and S3, a pattern consistent with the site exposure conditions described in Table 1 and examined further in Section 3.2.

3.2 Seasonal dynamics of sediment properties

Gypsum dissolution rates were significantly positively correlated with mean monthly wind speed at all three sites (S1: r = 0.81, $p < 0.001$; S2: r = 0.78, $p < 0.001$; S3: r = 0.85, $p < 0.001$), validating their use as proxy indicators of monthly mean hydrodynamic intensity. Gypsum dissolution rates exhibited pronounced seasonal variation at all three sites, with winter peaks and summer minima consistent with the seasonal wind environment (Supplementary Table S1). Winter peak dissolution rates reached 5.3, 7.9, and 11.3 g d^{-1} in bare areas at S1, S2, and S3, respectively, and declined to summer minima of 2.8, 4.9, and 7.2 g d^{-1}, confirming the hydrodynamic exposure gradient among the three sites. Dissolution rates in vegetated areas were consistently lower than in bare areas at all sites throughout the year, with annual mean reductions of 18%, 21%, and 25% at S1, S2, and S3, respectively, reflecting the attenuation of near-bed hydrodynamic energy by the seagrass canopy. The magnitude of this vegetated–bare difference was

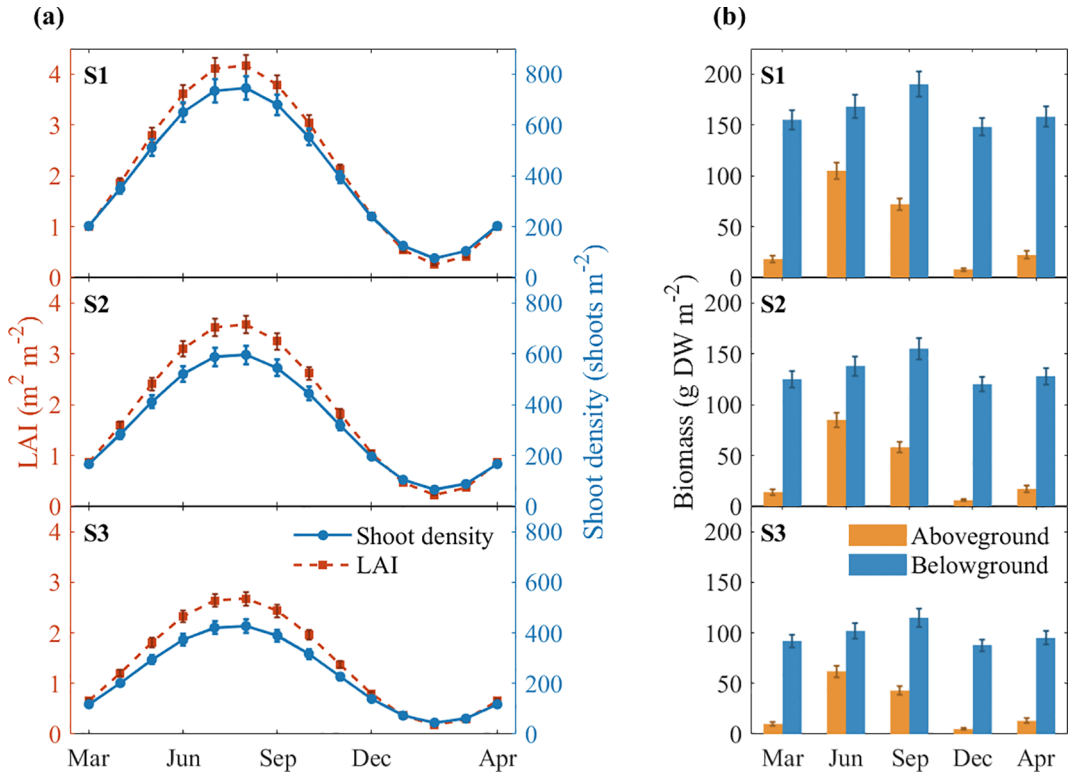


FIGURE 2
Seasonal dynamics of eelgrass meadow structure at three sites in the Yellow Sea. **(a)** Monthly variation in shoot density (filled circles, right axis) and leaf area index (LAI; filled squares, left axis). **(b)** Seasonal variation in aboveground and belowground biomass from quarterly sampling (March, June, September, December, and April of the following year). S1: Jiaozhou Bay (low-energy); S2: Huiquan Bay (intermediate-energy); S3: Laoshan Bay (high-energy). Data are mean ± standard error (SE); n = 5 replicate quadrats per site in **(a)**, n = 3 replicate quadrats per site in **(b)**.

greater in summer when canopy density was highest and smaller in winter following leaf senescence.

D50 in vegetated areas at all three sites exhibited significant seasonal oscillations, with finer sediment in summer and coarser sediment in winter; the seasonal oscillation amplitude in bare areas was substantially smaller than in vegetated areas (Figure 3). The peak-to-trough difference in vegetated D50 was 49, 50, and 44 μm at S1, S2, and S3, respectively, compared with only 13, 17, and 28 μm in bare areas. D50 in vegetated areas was lower than at the corresponding bare site in every month throughout the year. The difference between them (ΔD50) peaked in summer (July–August) at 55, 47, and 29 μm at S1, S2, and S3, respectively, and declined to minima in winter (December–January) at S1: 17 μm, S2: 13 μm, and S3: 11 μm. After controlling for hydrodynamic energy (gypsum dissolution rate) and benthic microalgal biomass (chlorophyll a), the treatment effect remained robust with a coefficient change of approximately 5%, indicating that the seasonal pattern of ΔD50 was not substantially influenced by these covariates (Supplementary Figure S1).

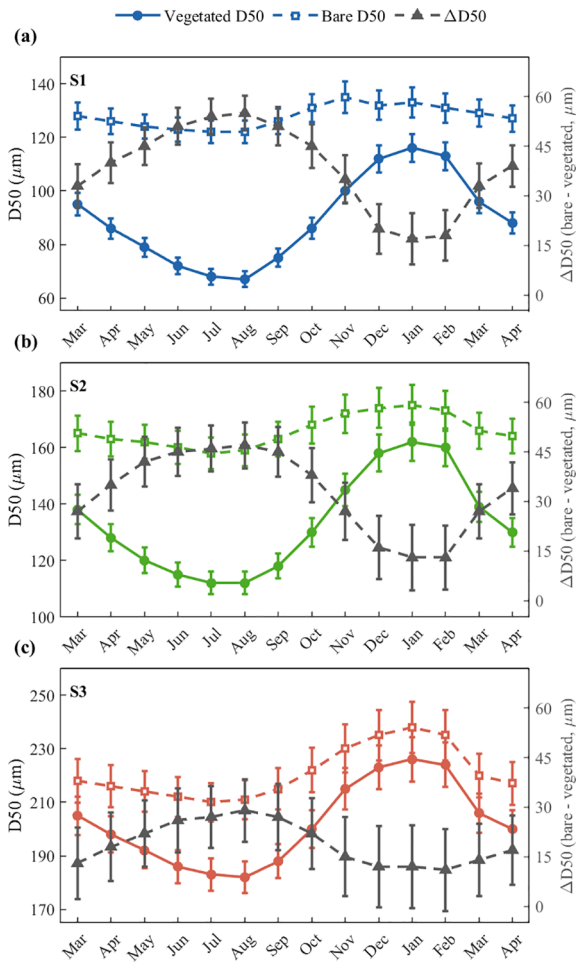


FIGURE 3
Seasonal dynamics of sediment median grain size (D50) in eelgrass meadow and bare sediment areas at three sites in the Yellow Sea. Left axis: mean ± 1 SE (n = 5) D50 in vegetated areas (green solid line) and bare areas (brown solid line). Right axis: their difference ΔD50 (dark grey dashed line). S1: Jiaozhou Bay (low-energy); S2: Huiquan Bay (intermediate-energy); S3: Laoshan Bay (high-energy).

Net deposition/erosion rates were in strong agreement with the seasonal pattern of D50 (Figures 4a–c). Vegetated areas at all three sites showed net deposition in summer (July–September), with peak rates of +2.3, +1.5, and +0.9 mm month^{-1} at S1, S2, and S3, respectively, transitioning to slight net erosion or near-zero conditions in winter. Winter net erosion rates in bare areas increased along the exposure energy gradient, with trough values of −1.1, −1.6, and −2.1 mm month^{-1} at S1, S2, and S3, respectively. Cumulative elevation trajectories further revealed the geomorphic effect at the 14-month scale (Figure 4d): vegetated areas showed net deposition of approximately +11 mm at S1, + 7 mm at S2, and near-zero at S3; bare areas showed net erosion of approximately −3 mm at S1, −6 mm at S2, and −9 mm at S3, with elevation loss most pronounced at the high-energy site.

Key parameter values across sites and seasons are summarized in Table 2.

3.3 Seasonal dynamics of benthic microalgae

Benthic chlorophyll a content exhibited significant seasonal oscillations at all three sites, peaking in summer (August–September) and reaching minimum values in winter (January–February) (Figures 5a–c). Peak values in vegetated areas were 112, 91, and 66 mg m^{-2} at S1, S2, and S3, respectively, declining to minima of 22, 18, and 13 mg m^{-2}, representing a seasonal oscillation amplitude of approximately fivefold. The timing of the benthic chlorophyll a peak lagged the *Z. marina* aboveground biomass peak (July–August) by approximately one month, indicating that although the two seasonal rhythms were similar, they were not perfectly synchronous. Benthic chlorophyll a content in vegetated areas was slightly higher than in bare areas at all sites (difference approximately 15–25%), suggesting that the reduction in near-bed flow velocity by the *Z. marina* canopy favoured microalgal colonisation.

LMM results indicated that benthic chlorophyll a had a significant negative correlation with D50 (standardised coefficient = −0.18, $p < 0.01$), but its effect size was only 51% of that of the treatment main effect (−0.35; Figure 5d). After controlling for the benthic chlorophyll a covariate, the vegetated-area treatment effect remained significant with a coefficient change of approximately 5%, indicating that the seagrass sediment stabilization effect was independent of the benthic microalgal contribution and could not be explained by seasonal variation in benthic microalgae.

3.4 Seasonal dynamics of water transparency and SPM

Secchi depth in vegetated areas was higher than in bare areas in every month throughout the year at all three sites. The transparency difference (ΔSecchi) peaked in summer (July–August), reaching 1.2, 0.9, and 0.6 m at S1, S2, and S3, respectively, and declined to winter minima (January–February) of 0.4 m at S1, 0.2 m at S2, and 0.1 m at S3 (Figures 6a–c). Absolute Secchi depth showed a pronounced site gradient, with summer peak values in vegetated areas of 3.1 m at S1, 2.3 m at S2, and 1.6 m at S3, reflecting the higher baseline water clarity at the low-energy site. The seasonal patterns of ΔSecchi were

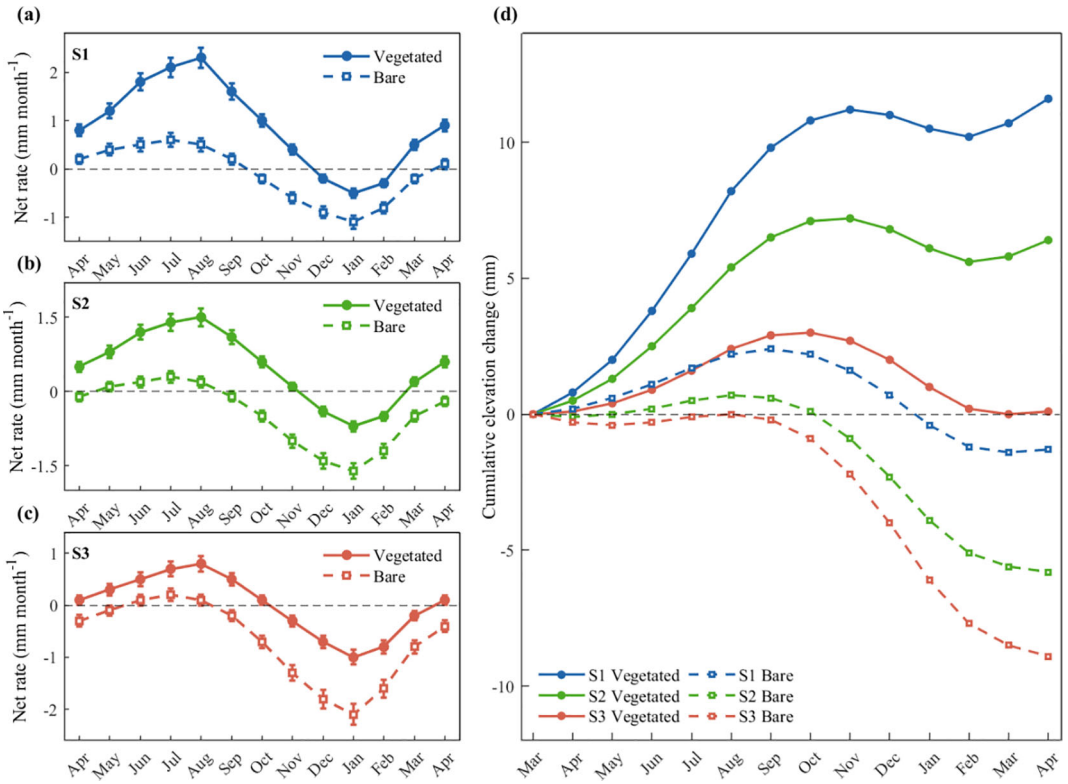


FIGURE 4
Seasonal variation in sediment dynamics in vegetated and bare areas at three sites in the Yellow Sea. **(a–c)** Monthly mean net deposition/erosion rates (mm month^{-1}) at each site; positive values indicate net deposition, negative values net erosion; error bars are ± 1 SE (n = 5). **(d)** Cumulative elevation change curves relative to the study start month (March 2024) as a zero baseline; solid lines are vegetated areas, dashed lines are bare areas, with colours distinguishing sites.

highly synchronous with ΔD50 (Figure 6) and LAI (Figure 2). Monthly mean transparency differences were strongly and positively correlated with LAI (S1: $R^2 = 0.89$; S2: $R^2 = 0.84$; S3: $R^2 = 0.77$; all $p < 0.001$), indicating that greater seagrass biomass corresponded to more substantial improvement in the water optical environment. These correlations were calculated using monthly ΔSecchi (vegetated minus bare) as the response variable and monthly mean LAI in the vegetated area as the predictor, with each site analysed separately (n = 14 months per site).

SPM concentration showed a seasonal pattern opposite to transparency, with all three sites exhibiting winter highs and summer lows (Figures 6d–f). SPM in vegetated areas was lower than in bare areas throughout the year. The SPM difference (ΔSPM) was also greatest in summer, with peak values of 9, 12, and 14 mg L^{-1} at S1, S2, and S3, respectively, narrowing to 6, 8, and 10 mg L^{-1} in winter. Winter peak SPM in bare areas increased along the exposure energy gradient, reaching 26, 34, and 45 mg L^{-1} at S1, S2, and S3, respectively, with particulate matter resuspension most intense at

TABLE 2 **Summary of key sediment and water optical parameters at three sites.**

Parameter	Season	S1	S2	S3
ΔD50 (μm)	Summer peak	55	47	29
ΔD50 (μm)	Winter minimum	17	13	11
Peak net deposition rate, Veg (mm month^{-1})	Summer	+2.3	+1.5	+0.9
Trough net erosion rate, Bare (mm month^{-1})	Winter	−1.1	−1.6	−2.1
Cumulative elevation change, Veg (mm)	14-month	+11	+7	≈0
Cumulative elevation change, Bare (mm)	14-month	−3	−6	−9
ΔSecchi (m)	Summer peak	1.2	0.9	0.6
ΔSecchi (m)	Winter minimum	0.4	0.2	0.1
ΔSPM (mg L^{-1})	Summer peak	9	12	14
ΔSPM (mg L^{-1})	Winter minimum	6	8	10
SPM in bare area (mg L^{-1})	Winter peak	26	34	45

ΔD50, bare minus vegetated; ΔSecchi, vegetated minus bare; ΔSPM, bare minus vegetated.

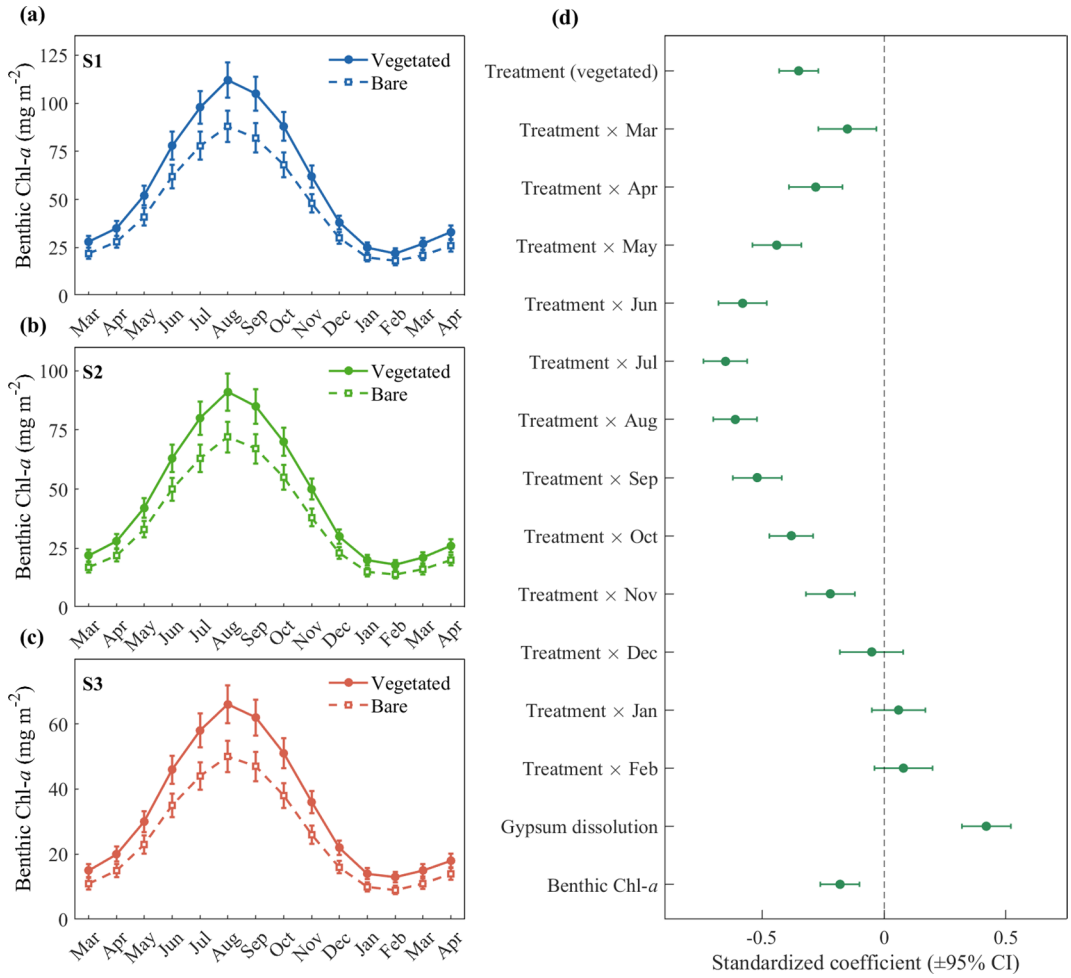


FIGURE 5
Seasonal dynamics of benthic microalgae and their relationship to sediment stabilization effects at three sites in the Yellow Sea. **(a–c)** Monthly time series of benthic chlorophyll a content (mg m^{-2}) in vegetated areas (solid lines) and bare areas (dashed lines); error bars are ± 1 SE (n = 5). **(d)** Standardised coefficients (± 95% CI) of fixed effects in the linear mixed-effects model (LMM) for sediment D50. Treatment (vegetated) is the main treatment effect of the vegetated area, Treatment × Month is the interaction effect between treatment and month, Gypsum dissolution rate and Benthic Chl-a are covariates.

the high-energy S3 site. The seasonal patterns of ΔSPM and ΔSecchi were in agreement (both greater in summer and smaller in winter), indicating that the improvement in water transparency in vegetated areas was directly attributable to the suppression of particulate matter resuspension by the sediment stabilization effect rather than to differences in algal-derived turbidity.

4 Discussion

4.1 Inferential significance of temporal dynamics evidence for causal direction

The difference in D50 between vegetated and bare areas (ΔD50) oscillated in strict synchrony with the seasonal rhythm of *Z. marina* aboveground biomass throughout the 14-month observation period: the difference widened as biomass increased and narrowed as biomass declined, with summer peak values of 55, 47, and 29 μm at the three sites and winter minima of 17, 13, and 11 μm. The seasonal peak-to-trough range in vegetated-area D50 (S1: 49 μm) far exceeded the self-oscillation amplitude of bare-area D50 (S1: 13 μm). This temporal coupling pattern has direct inferential significance for causal direction: if fine-grained substrate were passively attracting seagrass colonisation, substrate state should be relatively independent of seasonal biomass variation and should not oscillate systematically with the biomass rhythm. The observed strict synchrony is highly consistent with the direction of seagrass actively driving sediment change. Van der Heide et al. (2007) noted that cross-sectional designs are fundamentally incapable of distinguishing the two opposite causal directions between seagrass and sediment; the 14-month temporal dynamics evidence of the present study addresses this methodological limitation within an observational framework, advancing causal attribution from static association to testing at the level of temporal dynamics. After controlling for monthly mean hydrodynamic intensity (gypsum dissolution rate) and benthic microalgal biomass (chlorophyll a), the treatment effect coefficient changed by approximately 5%, further excluding seasonal variation in physical background conditions and benthic biofilm effects as alternative explanations. Surface elevation change

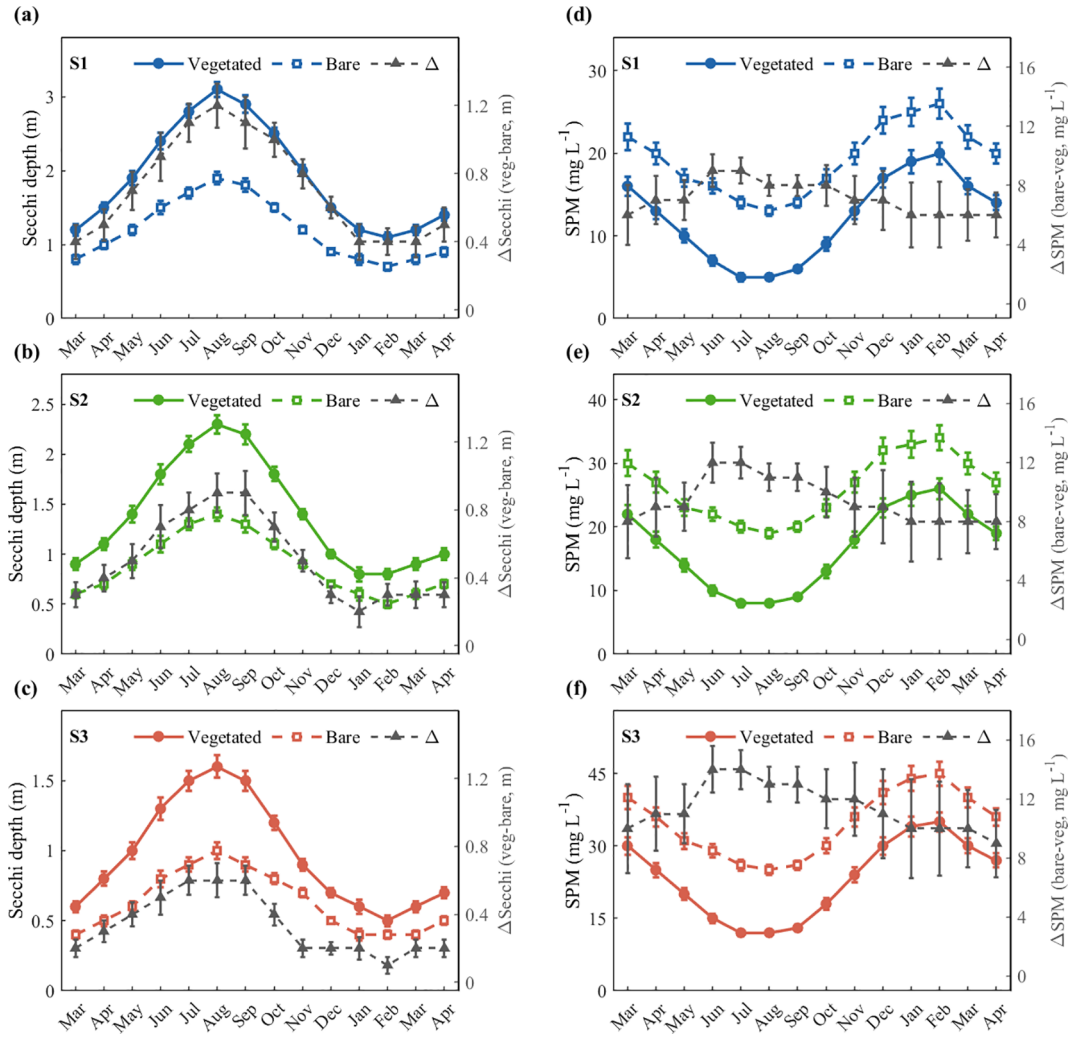


FIGURE 6
Seasonal dynamics of water optical environment and suspended particulate matter in vegetated and bare areas at three sites in the Yellow Sea. **(a–c)** Monthly time series of Secchi depth (m); left axis: mean ± 1 SE (n = 5) in vegetated areas (solid lines) and bare areas (dashed lines); right axis: their difference ΔSecchi (vegetated minus bare, dark grey dashed line). **(d–f)** Monthly time series of SPM concentration (mg L^{-1}); right axis: difference ΔSPM (bare minus vegetated). Blue, green, and red correspond to S1 (Jiaozhou Bay), S2 (Huiquan Bay), and S3 (Laoshan Bay), respectively.

pin (SECP) data provided independent validation at the geomorphic scale (Potouroglou et al., 2017): net deposition of +11 mm in the S1 vegetated area and net erosion of −3 mm in the bare area over 14 months, with trajectories in both seasonal rhythm and magnitude highly consistent with the ΔD50 pattern, indicating that the active seagrass effect on sediment has accumulated into measurable geomorphic mass-balance differences rather than merely transient fluctuations in surface grain size. The mechanistic sources producing this temporal pattern are analysed in detail below. It should be noted that the alternative hypothesis — that seagrass passively colonizes pre-existing fine-grained substrates — has limited empirical support in the literature, as seagrasses have been reported to preferentially colonize sandy substrates in some settings (Koch, 2001; Murphy et al., 2011). While this weakens the need to formally reject the passive-selection hypothesis, the temporal-dynamics approach adopted here offers broader methodological value beyond this specific dichotomy. By demonstrating that ΔD50 tracks biomass continuously across 14 months with predictable seasonal amplitude modulation, our results establish a quantitative framework for assessing the real-time functional intensity of sediment stabilization — information that static cross-sectional comparisons cannot provide regardless of how causality is framed. This continuous temporal resolution reveals several insights not available from prior work: (1) the complementary seasonal roles of canopy and rhizome pathways can be disentangled through their distinct temporal signatures; (2) the systematic decrease in stabilization amplitude along the hydrodynamic gradient quantifies the physical limits of canopy effectiveness under increasing wave exposure; and (3) the convergence of minimum protection and maximum hydrodynamic forcing during winter identifies a specific temporal vulnerability window with direct management implications. These contributions extend beyond the active-versus-passive debate and provide a temporally explicit evidence base for evaluating meadow functional status and prioritizing conservation interventions.

4.2 Seasonal drivers of canopy effects and attribution of winter residual effects

The seasonal peak-to-trough range of vegetated-area D50 (S1: 49 μm) far exceeded the self-oscillation amplitude of bare-area D50 (S1: 13 μm), indicating that the seasonal profile of ΔD50 was primarily driven actively by the canopy rather than by changes in the physical background. This pattern is consistent with the canopy hydrodynamic attenuation mechanism described in the Introduction, whereby seasonal changes in leaf area modulate near-bed shear stress and thus the critical conditions for fine-particle deposition or resuspension (Zhu et al., 2021). Four-season continuous monitoring along the Virginia coast by Hansen and Reidenbach (2013) recorded the same pattern: the proportion of time that near-bed shear stress exceeded the critical resuspension threshold was approximately 55% in summer and rose to above 80% in winter, with effect intensity varying systematically with seasonal biomass oscillations — entirely consistent in direction with the present study. High-resolution near-bed velocity profile measurements by Reidenbach and Thomas (2018) further confirmed that bed-surface shear stress within the seagrass zone during high-biomass periods (0.004–0.034 Pa) was significantly below the critical resuspension threshold (0.04 Pa), while bare-area values continuously exceeded it — a mechanism consistent with the seasonal pattern of the present study.

The gypsum dissolution data from the present study provide further supporting evidence for this canopy-driven seasonal pattern. Dissolution rates in vegetated areas were 18–25% lower than in bare areas on annual average, and this difference was most pronounced during summer when canopy density was highest. At the wave-dominated S2 and S3 sites, wind-generated waves were the primary driver of sediment resuspension, whereas tidal currents played a relatively greater role at the sheltered S1 site. Winter monsoon events generated the highest dissolution rates at all sites, with S3 bare-area rates reaching 11.3 g d^{-1}, corresponding to the period of greatest erosion vulnerability identified by the surface elevation data.

However, when winter aboveground biomass declined to its annual minimum (S1: 8 g DW m^{-2}), ΔD50 did not reach zero but narrowed to 17 μm before maintaining a non-zero residual. This residual effect must first be evaluated against the potential contribution of benthic microalgae: LMM results showed a standardised coefficient of −0.18 for benthic chlorophyll a, with an effect size only 51% of the treatment main effect (−0.35), and benthic chlorophyll a was at its annual minimum in winter (S1: approximately 22 mg m^{-2}); microalgae thus lacked the capacity to explain this residual in winter when the canopy had nearly disappeared. Having excluded microalgae, belowground biomass provides a more compelling explanatory source: winter belowground biomass still maintained 75–80% of peak values (S1: approximately 143–152 g DW m^{-2}), with the three-dimensional anchoring structure of the rhizome network within the substrate remaining intact. The stabilization effect of rhizomes depends on physical presence rather than metabolic activity and can therefore operate independently and continuously after canopy senescence. Conversely, Tassone et al. (2024) demonstrated that complete vegetation removal leads to rapid substrate coarsening, underscoring the critical role of both above- and belowground seagrass structures in maintaining sediment conditions. The most direct field evidence was provided by Potouroglou et al. (2017) from perennial *Z. marina* meadows in Scotland: vegetated-area elevation remained stable in winter when aboveground biomass was sparse, while the bare control showed evident seasonal erosion, with the explicit conclusion that "canopy biomass and morphology alone are insufficient to explain sediment retention, and the belowground effect of rhizomes is equally important." Controlled field manipulation experiments by Christianen et al. (2013) also confirmed that seagrass with severely grazed canopies (aboveground biomass only approximately 10 g m^{-2}) still reduced erosion threefold, attributed to the continuous anchoring effect of belowground biomass. Flume experiments by Marin-Diaz et al. (2020) further quantified that rhizome networks can reduce bedload transport by approximately 50%, and Infantes et al. (2022) measured reductions in lateral sediment erosion rates of up to 70% attributable to roots. Taken together, the complete seasonal profile of stabilization effects observed in the present study is consistent with the mechanistic picture of canopy hydrodynamic effects continuously modulating effect intensity with the biomass rhythm, and rhizome mechanical anchoring maintaining a non-zero baseline through winter. It is worth noting that existing studies are almost entirely based on single-season sampling; Dahl et al. (2020) explicitly noted that single-season sampling may lead to systematic overestimation of annual mean carbon stocks — a logical bias equally applicable to assessments of sediment stabilization function. Full-year continuous tracking is a necessary condition for accurately estimating annualised function (Zhu et al., 2022).

4.3 Synchronous transmission of sediment stabilization effects to the water optical environment

Differences in Secchi depth (ΔSecchi) and SPM concentration (ΔSPM) between vegetated and bare areas were positive in every month throughout the year. Both were highly coupled with the seasonal rhythm of LAI: correlation coefficients between ΔSecchi and LAI reached R^2 = 0.77–0.89 ($p < 0.001$), and the seasonal patterns of ΔSPM and ΔSecchi corresponded fully, both showing greater values in summer and smaller values in winter. SPM is the dominant factor controlling light attenuation and Secchi depth in coastal waters (Devlin et al., 2008), so the synchronous seasonal patterns of the two variables indicate that the improvement in water transparency in vegetated areas was directly attributable to the suppression of particulate matter resuspension by the sediment stabilization effect rather than to differences in algal-derived turbidity. The sediment–light coupled seasonal response was clearly observable at all three sites under contrasting hydrodynamic backgrounds.

It is noteworthy that the site-gradient direction of ΔSPM was opposite to that of ΔD50 and ΔSecchi: the summer peak of ΔSPM at S3 (14 mg L^{-1}) exceeded that at S1 (9 mg L^{-1}), while ΔD50 (29 μm) and ΔSecchi (0.6 m) at S3 were both lower than at S1. This does not indicate stronger stabilization effects at the high-energy site; rather, it reflects site differences in baseline SPM at bare areas, where winter

peak SPM at the S3 bare area reached 45 mg L^{-1}, nearly twice that at S1 (26 mg L^{-1}), mechanically inflating absolute differences. ΔD50 and ΔSecchi, as relative indices reflecting the degree of substrate grain size refinement and improvement in water transparency, more faithfully represent how effect intensity varies along the hydrodynamic gradient. The winter narrowing of stabilization effects (S1 ΔSecchi declining to 0.4 m), combined with the seasonal reduction in baseline light availability due to shorter day length and lower solar elevation angle, may impose a dual light limitation pressure on the carbon balance of overwintering rhizomes: Wong et al. (2020) showed that reduced autumn light causes *Z. marina* to consume large amounts of rhizome carbohydrate reserves, substantially increasing vulnerability entering winter; Staehr and Borum (2011) demonstrated that even with seasonal metabolic acclimation and a lowered winter light compensation point, severe light limitation could not be entirely overcome (Xu et al., 2020). These inferences, however, await future validation through direct measurement of benthic irradiance.

4.4 Two-tier modulation of stabilization effect seasonal dynamics by hydrodynamic exposure gradient

Peak aboveground biomass at the high-energy S3 site (62 g DW m^{-2}) was only 46% of that at the low-energy S1 site (105 g DW m^{-2}), and the summer peak ΔD50 at S3 (29 μm) was only 53% of that at S1 (55 μm). The seasonal oscillation amplitude of stabilization effects decreased systematically along the exposure energy gradient. This reflects the compressive effect of hydrodynamic exposure on the upper limit of effect intensity: high-energy environments directly compress the maximum attainable canopy effect magnitude by constraining biomass accumulation. *In situ* flume experiments by de Smit et al. (2022) demonstrated a linear positive relationship between the critical flow velocity for *Z. marina* sediment resuspension and leaf area, such that constrained biomass directly compresses the effect ceiling. A systematic survey of 53 *Z. marina* meadows by Dahl et al. (2020) further revealed that the dominant stabilization mechanism shifts from fine-particle trapping in sheltered environments to substrate compaction and erosion resistance in exposed environments — a mechanistic distinction of fundamental nature. This mechanistic distinction is independently supported by multiple experimental studies: flume experiments by Marin-Diaz et al. (2020) explicitly separated the functional division between canopy (reducing suspended re-deposition) and rhizomes (reducing bedload transport); Infantes et al. (2022) demonstrated that roots reduced cliff erosion by 70% in sandy (typical high-exposure) substrates but showed no significant effect in muddy (typical sheltered) substrates. Together, these studies established a mechanistic basis for the difference in stabilization mode between exposed and sheltered environments, although other factors — including biogeochemical differences and water temperature gradients — may also contribute to site-level variation. It should be noted that the three sites S1, S2, and S3 show systematic covariation between substrate type (silt–fine sand to medium sand) and wave energy, as confirmed by the gypsum dissolution rate gradient across sites (Supplementary Table S1), making it impossible to fully separate whether biomass differences are primarily driven by wave energy or baseline substrate conditions in the present study design; interpretation of site-gradient effects requires acknowledgement of this confounding.

Simultaneously, the hydrodynamic exposure gradient creates a second tier of modulation by amplifying geomorphic vulnerability. The winter net erosion rate in bare areas at S3 was highest (−2.1 mm $month^{-1}$), with a cumulative elevation loss of −9 mm over 14 months — three times that at S1 bare areas (−3 mm). The cumulative elevation in the S3 vegetated area was near zero over 14 months, poised between weak protection and intense erosion, already approaching geomorphic mass-balance equilibrium. Walter et al. (2020) documented large-scale irreversible erosion following collapse of *Z. marina* at estuary scale in Morro Bay, California — more than 90% of the former seagrass area eroded, with maximum elevation losses of 0.50 m and a transition of the entire estuary from a depositional to an erosional regime — providing the most direct empirical evidence that cover loss triggers difficult-to-reverse net erosion. Research by El-Hacen et al. (2019) across an exposure gradient in Mauritania similarly indicated stronger coupling between geomorphic stability and vegetation cover state at high-exposure sites, where any cover loss may trigger a state shift beyond a critical threshold (Maxwell et al., 2017). The superposition of both tiers carries an important ecological implication: the active seagrass effect on sediment is weakest at high-energy sites, the meadow itself is already near geomorphic equilibrium, and the erosion cost of its absence is greatest. During winter, both pressures are most concentrated — minimum seasonal biomass (weakest driving capacity) coincides with strengthened monsoon winds and highest external erosion pressure — making winter at high-energy sites the most vulnerable window for geomorphic stability throughout the year.

4.5 Conservation management implications and study limitations

The results of the present study have clear practical implications for nearshore seagrass conservation management. Winter is the period when the capacity of seagrass to actively drive sediment stabilization is most broadly weakest and erosion risk in bare areas is highest, with high-energy sites particularly prominent. Human activities that may cause seagrass cover loss — including dredging, aquaculture expansion, and navigation channel maintenance — should be prioritised for avoidance of the winter window period. High-exposure sites, combining the weakest effect with the highest vulnerability, warrant priority protection at the full annual scale; should cover loss occur, rapid restoration intervention should be prioritised to prevent the establishment of net-erosion trajectories.

Several limitations of the present study should be acknowledged. First, in the observational paired design, the reverse causality of fine-grained substrate favouring seagrass colonisation, while incompatible with the seasonal dynamics evidence, cannot be theoretically excluded entirely by this study design; final verification requires transplantation experiments (Bos et al., 2007; Orth et al., 2020) or historical remote-sensing reconstruction. Second, canopy-interior flow velocity and rhizome mechanical metrics were not

directly measured; quantitative partitioning of the contributions of canopy and rhizome effects to the full-year stabilization profile depends on future removal-control experiments (Tassone et al., 2024; Dahl et al., 2021). Third, hydrodynamic conditions were characterized using gypsum dissolution rates as a proxy rather than direct measurements of current velocity, wave height, or bed shear stress. Although the gypsum proxy was well correlated with wind speed (r = 0.78–0.85) and effectively captured the hydrodynamic gradient and seasonal variation among sites, it cannot resolve event-scale dynamics or distinguish the relative contributions of tidal currents and waves to bed shear stress. Future studies would benefit from incorporating direct hydrodynamic measurements or validated parametric wave models to provide a more complete physical context for interpreting sediment dynamics. Fourth, site-specific sediment bulk density was not measured; surface elevation changes therefore represent vertical accretion or erosion rather than mass fluxes. Future studies should incorporate direct bulk density measurements to enable quantitative mass-balance calculations. Fifth, substrate type and hydrodynamic energy are systematically covarying across the three sites; mechanistic attribution of site-gradient effects requires future verification through controlled substrate conditions. Sixth, the statistical power of the 14-month time series is limited; longer time series will further strengthen the robustness of temporal dynamics evidence. Seventh, the study area was confined to the temperate *Z. marina* population along the Qingdao coast of the Yellow Sea; extrapolation of conclusions to other climate zones, seagrass species, or tidal regimes should be made with caution.

5 Conclusions

This study systematically documented the full-year temporal dynamics of seagrass-mediated sediment stabilization through 14 consecutive months of paired field observations at three sites along a hydrodynamic exposure gradient in the Yellow Sea. Three principal conclusions emerge.

First, the difference in sediment grain size between vegetated and bare areas (ΔD50) followed the seasonal rhythm of *Zostera marina* aboveground biomass continuously and strictly, and this pattern remained robust after controlling for hydrodynamic intensity and benthic microalgal biomass. This temporal coupling advances the causal attribution of seagrass sediment stabilization from static cross-sectional association to temporal-dynamics-level evidence, effectively addressing the long-standing inability of single-time-point designs to distinguish active seagrass driving from passive substrate selection. A non-zero winter residual ΔD50 coincided with persistent belowground biomass, indicating that canopy and rhizome effects play complementary seasonal roles — the canopy modulates effect intensity with the biomass rhythm while rhizome anchoring maintains a baseline through winter.

Second, water transparency differences between vegetated and bare areas were strongly coupled with leaf area index across all three sites, demonstrating that sediment stabilization simultaneously improves the benthic light environment. This sediment–light coupled seasonal response provides observational evidence for a positive feedback mechanism that may contribute to meadow self-maintenance.

Third, the seasonal amplitude of stabilization effects decreased systematically with increasing hydrodynamic exposure, while winter erosion vulnerability in bare areas was greatest at the high-energy site. The convergence of weakest protection and highest vulnerability identifies winter at high-exposure meadows as the most critical management window. Anthropogenic disturbances that risk cover loss should be prioritized for avoidance during this period, and high-exposure meadows warrant year-round priority protection.

Data availability statement

The original contributions presented in the study are included in the article/Supplementary Material, further inquiries can be directed to the corresponding author/s.

Author contributions

LC: Conceptualization, Data curation, Formal analysis, Investigation, Methodology, Writing – original draft, Writing – review & editing. XL: Investigation, Writing – review & editing. AZ: Investigation, Writing – review & editing. XW: Investigation, Writing – review & editing. JL: Conceptualization, Supervision, Writing – review & editing.

Funding

The author(s) declared that financial support was not received for this work and/or its publication.

Acknowledgments

The authors thank the editorial team and the anonymous reviewers for their insightful comments on the article.

Conflict of interest

The author(s) declared that this work was conducted in the absence of any commercial or financial relationships that could be construed as a potential conflict of interest.

Generative AI statement

The author(s) declared that generative AI was not used in the creation of this manuscript.

Any alternative text (alt text) provided alongside figures in this article has been generated by Frontiers with the support of artificial intelligence and reasonable efforts have been made to ensure accuracy, including review by the authors wherever possible. If you identify any issues, please contact us.

Publisher's note

All claims expressed in this article are solely those of the authors and do not necessarily represent those of their affiliated organizations, or those of the publisher, the editors and the reviewers. Any product that may be evaluated in this article, or claim that may be made by its manufacturer, is not guaranteed or endorsed by the publisher.

Supplementary material

The Supplementary Material for this article can be found online at: https://www.frontiersin.org/articles/10.3389/fmars.2026.1843359/full#supplementary-material.

References

Bartoń, K. (2023). *MuMIn: multi-model inference*. Available online at: https://CRAN.R-project.org/package=MuMIn (Accessed October 10, 2025).

Bates, D., Mächler, M., Bolker, B., and Walker, S. (2015). Fitting linear mixed-effects models using lme4. *J. Stat. Software* 67, 1–48. doi: 10.18637/jss.v067.i01

Bos, A. R., Bouma, T. J., de Kort, G. L. J., and van Katwijk, M. M. (2007). Ecosystem engineering by annual intertidal seagrass beds: sediment accretion and modification. *Estuar. Coast. Shelf Sci.* 74, 344–348. doi: 10.1016/j.ecss.2007.04.006

Christianen, M. J. A., van Belzen, J., Herman, P. M. J., van Katwijk, M. M., Lamers, L. P. M., van Leent, P. J. M., et al. (2013). Low-canopy seagrass beds still provide important coastal protection services. *PloS One* 8, e62413. doi: 10.1371/journal.pone.0062413

Dahl, M., Asplund, M. E., Björk, M., Deyanova, D., Infantes, E., Isaeus, M., et al. (2020). The influence of hydrodynamic exposure on carbon storage and nutrient retention in eelgrass (Zostera marina L.) meadows on the Swedish Skagerrak coast. *Sci. Rep.* 10, 13666. doi: 10.1038/s41598-020-70403-5

Dahl, M., Björk, M., and Gullström, M. (2021). Effects of seagrass overgrazing on sediment erosion and carbon sink capacity: current understanding and future priorities. *Limnol. Oceanogr. Lett.* 6, 309–319. doi: 10.1002/lol2.10211

de Smit, J. C., Bin Mohd Noor, M. S., Infantes, E., and Bouma, T. J. (2022). Wind exposure and sediment type determine the resilience and response of seagrass meadows to climate change. *Limnol. Oceanogr.* 67, S121–S132. doi: 10.1002/lno.11865

Devlin, M. J., Barry, J., Mills, D. K., Gowen, R. J., Foden, J., Sivyer, D., et al. (2008). Relationships between suspended particulate material, light attenuation and Secchi depth in UK marine waters. *Estuar. Coast. Shelf Sci.* 79, 429–439. doi: 10.1016/j.ecss.2008.04.024

Dunic, J. C., Brown, C. J., Connolly, R. M., Turschwell, M. P., and Côté, I. M. (2021). Long-term declines and recovery of meadow area across the world's seagrass bioregions. *Glob. Change Biol.* 27, 4096–4109. doi: 10.1111/gcb.15684

El-Hacen, E. M., Bouma, T. J., Govers, L. L., Piersma, T., and Olff, H. (2019). Seagrass sensitivity to collapse along a hydrodynamic gradient: evidence from a pristine subtropical intertidal ecosystem. *Ecosystems* 22, 1007–1023. doi: 10.1007/s10021-018-0319-0

Ganthy, F., Sottolichio, A., and Verney, R. (2013). Seasonal modification of tidal flat sediment dynamics by seagrass meadows of Zostera noltii (Bassin d'Arcachon, France). *J. Mar. Syst.* 109–110, S233–S240. doi: 10.1016/j.jmarsys.2011.11.027

Hansen, J. C. R., and Reidenbach, M. A. (2013). Seasonal growth and senescence of a Zostera marina seagrass meadow alters wave-dominated flow and sediment suspension within a coastal bay. *Estuar. Coasts* 36, 1099–1114. doi: 10.1007/s12237-013-9620-5

Infantes, E., Hoeks, S., Adams, M. P., van der Heide, T., van Katwijk, M. M., and Bouma, T. J. (2022). Seagrass roots strongly reduce cliff erosion rates in sandy sediments. *Mar. Ecol. Prog. Ser.* 700, 1–12. doi: 10.3354/meps14196

Koch, E. M. (2001). Beyond light: physical, geological and geochemical parameters as possible submersed aquatic vegetation habitat requirements. *Estuaries* 24, 1–17. doi: 10.2307/1352808

Léger-Daigle, R., Noisette, F., Bélanger, S., Cusson, M., and Nozais, C. (2022). Photoacclimation and light thresholds for cold temperate seagrasses. *Front. Plant Sci.* 13, 805065. doi: 10.3389/fpls.2022.805065

Lenth, R. V. (2023). "emmeans: Estimated Marginal Means, aka Least-Squares Means," in *R package version 1.8.7.* (Comprehensive R Archive Network (CRAN)). Available online at: https://CRAN.R-project.org/package=emmeans (Accessed October 10, 2025).

Lima, M. A. C., Bergamo, T. F., Ward, R. D., and Joyce, C. B. (2023). A review of seagrass ecosystem services: providing nature-based solutions for a changing world. *Hydrobiologia* 850, 2655–2670. doi: 10.1007/s10750-023-05244-0

Marin-Diaz, B., Bouma, T. J., and Infantes, E. (2020). Role of eelgrass on bed-load transport and sediment resuspension under oscillatory flow. *Limnol. Oceanogr.* 65, 426–436. doi: 10.1002/lno.11312

Maxwell, P. S., Eklöf, J. S., van Katwijk, M. M., O'Brien, K. R., de la Torre-Castro, M., Boström, C., et al. (2017). The fundamental role of ecological feedback mechanisms for the adaptive management of seagrass ecosystems — a review. *Biol. Rev.* 92, 1521–1538. doi: 10.1111/brv.12294

McKenzie, L. J., Nordlund, L. M., Jones, B. L., Cullen-Unsworth, L. C., Roelfsema, C., and Unsworth, R. K. F. (2020). The global distribution of seagrass meadows. *Environ. Res. Lett.* 15, 074041. doi: 10.1088/1748-9326/ab7d06

Mohr, V., Zhang, W., Dolch, T., and Schrum, C. (2025). The importance of seasonality in seagrass properties for coastal hydro-morphodynamics — a case study in a Wadden Sea basin. *J. Geophys. Res. Earth Surf.* 130, e2025JF008331. doi: 10.1029/2025JF008331

Murphy, R., Orzetti, L., and Johnson, W. (2011). *Plant fact sheet for eelgrass (Zostera marina L.)* (Beltsville, MD, USA: USDA Natural Resources Conservation Service, Norman A. Berg National Plant Materials Center).

Orth, R. J., Lefcheck, J. S., McGlathery, K. S., Aoki, L., Luckenbach, M. W., Moore, K. A., et al. (2020). Restoration of seagrass habitat leads to rapid recovery of coastal ecosystem services. *Sci. Adv.* 6, eabc6434. doi: 10.1126/sciadv.abc6434

Potouroglou, M., Bull, J. C., Krauss, K. W., Kennedy, H., Fusi, M., Daffonchio, D., et al. (2017). Measuring the role of seagrasses in regulating sediment surface elevation. *Sci. Rep.* 7, 11917. doi: 10.1038/s41598-017-12354-y

R Core Team (2023). *R: A language and environment for statistical computing* (Vienna, Austria: R Foundation for Statistical Computing).

Reidenbach, M. A., and Thomas, E. L. (2018). Influence of the seagrass, Zostera marina, on wave attenuation and bed shear stress within a shallow coastal bay. *Front. Mar. Sci.* 5, 397. doi: 10.3389/fmars.2018.00397

Reidenbach, M. A., and Timmerman, R. (2019). Interactive effects of seagrass and the microphytobenthos on sediment suspension within shallow coastal bays. *Estuar. Coasts* 42, 2038–2053. doi: 10.1007/s12237-019-00627-w

Staehr, P. A., and Borum, J. (2011). Seasonal acclimation in metabolism reduces light requirements of eelgrass (Zostera marina). *J. Exp. Mar. Biol. Ecol.* 407, 139–146. doi: 10.1016/j.jembe.2011.05.031

Tassone, S. J., Ewers Lewis, C. J., McGlathery, K. J., and Pace, M. L. (2024). Seagrass ecosystem recovery: experimental removal and synthesis of disturbance studies. *Limnol. Oceanogr.* 69, 1593–1605. doi: 10.1002/lno.12608

van der Heide, T., van Nes, E. H., Geerling, G. W., Smolders, A. J. P., Bouma, T. J., and van Katwijk, M. M. (2007). Positive feedbacks in seagrass ecosystems: implications for success in conservation and restoration. *Ecosystems* 10, 1311–1322. doi: 10.1007/s10021-007-9099-7

Walter, R. K., O'Leary, J. K., Vitousek, S., Taherkhani, M., Geraghty, C., and Kitajima, A. (2020). Large-scale erosion driven by intertidal eelgrass loss in an estuarine environment. *Estuar. Coast. Shelf Sci.* 243, 106910. doi: 10.1016/j.ecss.2020.106910

Wang, Z. H., Ma, Q. F., Liang, S. X., Liu, Y. A., Liu, L. M., Huang, C., et al. (2024). Study on the distribution and habitat suitability of seagrass in the Northern Chinese Seas. *Front. Mar. Sci.* 10, 1297137. doi: 10.3389/fmars.2023.1297137

Wong, M. C., Griffiths, G., and Vercaemer, B. (2020). Seasonal response and recovery of eelgrass (Zostera marina) to short-term reductions in light availability. *Estuar. Coasts* 43, 120–134. doi: 10.1007/s12237-019-00664-5

Xu, S. C., Wang, P. M., Wang, F., Liu, P., Liu, B. J., Zhang, X. M., et al. (2020). In situ responses of the eelgrass Zostera marina L. to water depth and light availability in the context of increasing coastal water turbidity: implications for conservation and restoration. *Front. Plant Sci.* 11, 582557. doi: 10.3389/fpls.2020.582557

Xu, S. C., Xu, S., Zhou, Y., Yue, S. D., Zhang, X. M., Gu, R. T., et al. (2021). Long-term changes in the unique and largest seagrass meadows in the Bohai Sea (China) using satellite, (1974–2019) and sonar data: implication for conservation and restoration. *Remote Sens.* 13, 856. doi: 10.3390/rs13050856

Zhang, P. D., Liu, Y. S., Guo, D., Li, W. T., and Zhang, Q. (2016). Seasonal variation in growth, morphology, and reproduction of eelgrass Zostera marina on the eastern coast of the Shandong Peninsula, China. *J. Coast. Res.* 32, 315–322. doi: 10.2112/JCOASTRES-D-14-00117.1

Zhu, Q., Wiberg, P. L., and McGlathery, K. J. (2022). Seasonal growth and senescence of seagrass alters sediment accumulation rates and carbon burial in a coastal lagoon. *Limnol. Oceanogr.* 67, 1931–1942. doi: 10.1002/lno.12178

Zhu, Q., Wiberg, P. L., and Reidenbach, M. A. (2021). Quantifying seasonal seagrass effects on flow and sediment dynamics in a back-barrier bay. *J. Geophys. Res. Oceans* 126, e2020JC016547. doi: 10.1029/2020JC016547